RSC Advances

PAPER

View Article Online
View Journal | View Issue

Cite this: *RSC Adv.*, 2021, **11**, 25274

High pressure polymorphism of $LiBH_4$ and of $NaBH_4$†

Adrien Marizy,[a] Grégory Geneste,[a] Gaston Garbarino[b] and Paul Loubeyre*[a]

Received 30th January 2021
Accepted 8th July 2021

DOI: 10.1039/d1ra00816a

rsc.li/rsc-advances

The pressure-induced structural changes in $LiBH_4$ and in $NaBH_4$ have been investigated experimentally up to 290 GPa by coupling Raman spectroscopy, infrared absorption spectroscopy and synchrotron X-ray diffraction. This data set is also analysed in the light of Density Functional Theory calculations performed up to 600 GPa. The $[BH_4]^-$ unit appears to be remarkably resistant under pressure. $NaBH_4$ remains stable in the known *Pnma* γ-phase up to 200 GPa and calculations predict a transition to a metallic polymeric *C2/c* phase at about 480 GPa. $LiBH_4$ is confirmed to exhibit a richer polymorphism. A new *Pnma* orthorhombic phase VI is found to be stable above 60 GPa and there are hints of a possible phase VII above 160 GPa. DFT calculations predict that two other high pressure $LiBH_4$ phases should appear at about 290 and 428 GPa. A very slight solubility of H_2 inside phases II, III and V of $LiBH_4$ is observed. A $NaBH_4(H_2)_{0.5}$ complex is predicted to be stable above 150 GPa.

Introduction

The unique potential of $LiBH_4$ and $NaBH_4$ for solid hydrogen storage is widely discussed in the literature, since these compounds could theoretically meet the 2025 DOE target for onboard hydrogen storage in terms of gravimetric and volumetric hydrogen densities (respectively 18.4 wt% and 122.5 kg H_2 per m^3 for $LiBH_4$ and 10.6 wt% and 113.1 kg H_2 per m^3 for $NaBH_4$). However, the strong covalent bond in the BH_4^- units of borohydrides requires a high decomposition temperature (>500 °C for $NaBH_4$ (ref. 1) and 380 °C for $LiBH_4$ (ref. 2)) which hampers their use in practical applications. A lot of chemical engineering work has already been done with some success,[3–10] through catalyst addition or nanotailoring, to try to lower their decomposition temperature but near-room-temperature hydrogen desorption/absorption has not been achieved yet. Therefore, it is of tremendous importance to continue to explore the possible mechanisms of destabilization of the boron–hydrogen bonds.

Recently, pressure has emerged as an effective means of producing new structures and materials, potentially interesting for hydrogen storage.[11–14] Indeed, the application of high pressure (>GPa) significantly reduces interatomic distances and thus modifies the chemical bonding, the molecular configuration and the crystal structure. More specifically, for borohydrides, a high pressure study is an effective way of producing new polymorphs with increased coordination numbers, new $[BH_4]^-$ anion charges, reduced H–H distances and mono/bi/tridentate configurations. Disclosing such effects should be useful to strengthen our understanding of the factors governing the B–H bond stability. Besides, the search for novel materials with targeted properties using Density Functional Theory (DFT) calculations has recently made tremendous progress. One way to evaluate the reliability of such calculations to explore the configuration space of the borohydrides family is to test them against the high pressure phase diagrams of selected compounds, such as $LiBH_4$ and $NaBH_4$. Finally, it has been demonstrated in many compounds that hydrogen uptake drastically increases under very high hydrogen pressure. Not only are interstitial hydrides more filled with hydrogen[15] but new polyhydrides[16,17] or hydrogen complexes such as $NH_3BH_3(H_2)_{1.5}$ are also created.[18,19] Hence, is it possible to insert more hydrogen into $LiBH_4$ and in $NaBH_4$? Even if the new dense polymorphs/hydrides found under pressure cannot be recovered at atmospheric pressure, a chemical substitution could then be attempted to stabilize them at ambient pressure.

The present work aims to experimentally and numerically extend the known phase diagrams of $NaBH_4$ and $LiBH_4$ up to the metallization pressure and to numerically explore the possibility of including more hydrogen inside $NaBH_4$. Sodium borohydride was studied at room temperature up to 90 GPa by X-ray diffraction and Raman spectroscopy with neon or hydrogen as a pressure medium and up to 200 GPa by infrared absorption spectroscopy without any pressure medium. $LiBH_4$ was studied at room temperature up to 130 GPa by X-ray diffraction in a helium pressure medium, by Raman spectroscopy up to 70 GPa and by IR absorption up to 290 GPa without any pressure medium. *Ab initio* calculations were conducted to complement the experimental investigation. The use of

[a]CEA, DAM, DIF, F-91297 Arpajon, France. E-mail: paul.loubeyre@cea.fr
[b]ESRF, The European Synchrotron, 71 Avenue des Martyrs, 38000 Grenoble, France

† Electronic supplementary information (ESI) available. See DOI: 10.1039/d1ra00816a

molecular dynamics simulations, in particular, has enabled us to discover a potential $NaBH_4(H_2)_{0.5}$ compound.

Current knowledge on the phase diagrams of $LiBH_4$ and $NaBH_4$

Many works have already explored the phase diagram of $NaBH_4$ and $LiBH_4$ up to the 50 GPa pressure range. At ambient pressure and temperature, $NaBH_4$ has a cubic phase (space group $Fm\bar{3}m$) in which the tetrahedral units $[BH_4]^-$ are disordered due to thermal agitation.[20–24] This structure was found to transform *via* a disorder–order transition into a tetragonal $P\bar{4}2_1c$ structure, either below 190 K at atmospheric pressure[21,25,26] or above 6 GPa at ambient temperature. A tetragonal to orthorhombic transition (space group *Pnma*) is observed at 9 GPa.[27–33] This experimental sequence of transitions was not initially predicted by DFT[27] but subsequent numerical studies accurately described it.[34–37] It should be noted that two nearly identical structures have been proposed experimentally for the tetragonal phase[26,38] and that calculations show that the most stable tetragonal structure is described in the higher symmetry $P4_2/nmc$ space group and not in the $P\bar{4}2_1c$ space group.[39] The last experimental work published on $NaBH_4$ suggests a monoclinic transition near 20 GPa due to anomalies in the evolution *versus* pressure of the B–H Raman vibrons.[32] Nevertheless, previous X-ray studies up to 30 GPa have not reported any monoclinic phase apparition.[28,30,31]

At room temperature and atmospheric pressure, the disordered cubic $Fm\bar{3}m$ structure is shared by all other univalent borohydrides but $LiBH_4$.[40] $LiBH_4$ has a richer polymorphism, as shown as early as 1974 by Pistorius[41] and slightly revised and refined 30 years later.[33,42–47] Its phase at ambient conditions (phase II) is a *Pnma* orthorhombic structure without disorder[48] and with undistorted $[BH_4]^-$ tetrahedra.[44,49] This phase transforms with slight hydrogen desorption (0.3 wt% (ref. 50)) into a hexagonal one at 381 K (phase I, space group $P6_3mc$).[44,48] Under pressure at ambient temperature, at 1 GPa, a new phase appears. It was first described in the *Ama*2 space group by Filinchuk *et al.*[45] and lately better described in the $I4_1/acd$ space group[46,51] (phase III). This phase was proven to be metastable down to atmospheric pressure below 200 K.[42,52] This phase III starts to transform into the well-known disordered cubic phase (phase V, $Fm\bar{3}m$) from 17 GPa at 300 K and at lower pressure if temperature is raised.[43] Nakano *et al.* identified that this transition was achieved through an intermediate tetragonal but also disordered phase V′, between 17 GPa and 30 GPa at room temperature.[46] The authors also pointed out that a significant weakening of the recorded XRD signal near 50 GPa probably portended a new phase transition. After this study, Yao & Klug used DFT calculations to predict two possible monoclinic candidate phases for phase VI with a $C2/m$ and a $C2/c$ (distorted NiAs) space group. $LiBH_4$ was also predicted to be metallic in a new polymeric monoclinic phase VII at 425 GPa.[51] Although the calculations accurately predicted that the tetrahedron would have an ideal geometry in phase II,[53] they also predict other structures for phases I and II, which are clearly at variance with the experimental data[54–57] or have later been contradicted.[58] Besides, several recent DFT studies are not accurate at high pressure either because they did not take into account the stable $I4_1/acd$ structure[59,60] or because they did not have enough atoms in their supercells to find it.[61]

It has to be pointed out that historically a PT domain between phase I and III was assigned to a new phase IV by Pistorius *et al.*[41] No new phase was found by synchrotron X-ray diffraction but a mixture of the two phases at the transition.[43] Hence, phase IV does not exist but the numeration remained unchanged. Therefore, in this study, the usual numeration will be kept.

Methods

Sample preparation

$NaBH_4$ and $LiBH_4$ samples were obtained from commercial Sigma-Aldrich powder with a purity of respectively 99% and 95%. Manipulations of the two borohydrides were made inside a high-purity argon glove box (H_2O < 1 ppm). After the loading of the samples inside the Diamond Anvil Cell (DAC), the DAC is manually closed tightly to avoid any water contamination outside the glovebox. Diamond anvil culets (300 μm, 150 μm, 100 μm or 40 μm in diameter) were used to cover various pressure domains. The rhenium gasket was covered with a 1000 Å thick layer of gold to ensure good airtightness prior to any loading with a pressure transmitting gas under 1400 bars. When no pressure medium was used (IR absorption measurements and Raman spectroscopy on $LiBH_4$), no gold was used on the gasket. When the DACs were loaded with gas, neon and hydrogen were used with a moisture content inferior to 2 ppm (Air Products Premier Line) for $NaBH_4$ and with helium with a moisture content inferior to 20 ppb (Air Products BIP Technology) for $LiBH_4$. Several purges/pumping cycles were done to dry all the gas loading device before the opening of the DAC for gas loading, especially for $LiBH_4$ because of its highly hygroscopic nature.

Sample characterisations

$LiBH_4$ and $NaBH_4$ are weak X-ray scatterers, which renders their high pressure structural characterisation in a DAC particularly challenging. X-ray diffraction measurements on $LiBH_4$ and $NaBH_4$ were performed at the ID27 beamline of the European Synchrotron Radiation Facility with a wavelength of 0.3738 Å, an X-ray beam of around 5 μm and a MAR-CCD detector. An XRD pattern of $LiBH_4$ at 68 GPa was also collected using a MAR555 detector on ID15b (0.4111 Å) for improved sensitivity. The pressure was measured using the equation of state of a small gold piece placed next to the sample for $LiBH_4$ and with the hydrostatic ruby pressure scale for $NaBH_4$. The X-ray diffraction patterns were analysed using DIOPTAS[62] and the FULLPROF software.[63] Uncertainties are estimated to be ±2% for pressure and ±0.2 $Å^3$ for volume.

Infrared absorption and Raman spectroscopy have been performed to complement the XRD structural investigation. First, discontinuities in the frequency shift *versus* pressure of

the various excitation modes of the BH_4 entity reflect the variation of the crystal field acting on it with high sensitivity. Therefore, they can reveal subtle structural changes that would be difficult to extract from XRD, such as a change of orientational order of the BH_4 tetrahedra. Besides, for spectroscopic studies, the size of the sample is much less problematic than for XRD and so IR absorption can be used to extend the structural investigation up to 200 GPa.

Infrared absorption spectroscopy was performed at room temperature using the synchrotron radiation source at the SMIS beamline of the French SOLEIL Synchrotron. The IR experimental configuration already described previously[64] includes a horizontal infrared microscope made up of two Schwarzschild objectives (×15, N.A. 0.5, W.D. = 43 mm) producing a 22 μm (FWHM) IR spot. Spectra were taken with a 4 cm^{-1} resolution with 512 accumulations. The high-frequency edge of the T_{2g} Raman band of the diamond anvil was used to estimate the pressure according to Akahama's calibration.[65]

Confocal Raman spectroscopy was performed using an Alpha300M+ (Witec) spectroscopic system with a continuous Ar–Kr laser emitting at 488.0 nm. The Stokes Raman signal was collected in back-scattering geometry by a CCD coupled to a 600 g mm^{-1} grating.

Ab initio calculations

Ab initio calculations have been performed to guide the discussion of the experimental data with insights at a microscopic level. We have performed DFT calculations using the Generalized Gradient Approximation in the form proposed by Perdew, Burke and Ernzerhof (GGA-PBE).[66] We have used the ABINIT code.[67] Four kinds of calculations have been performed: first, structural optimizations under fixed pressure; second, phonon calculations in the framework of the Density-Functional Perturbative Theory (DFPT);[68,69] third Molecular Dynamics (MD) runs in the isothermal–isobaric (NPT) ensemble; fourth constrained *Ab Initio* Random Structure Searching (AIRSS).[70]

The structural optimizations have been done in the Projector Augmented Wave (PAW) framework, with a plane-wave (PW) cut-off of 40 Hartrees, and a 6 × 6 × 6 *k*-point mesh for insulating phases and 12 × 12 × 12 *k*-point mesh for metallic phases. All the non-disordered experimental or predicted stable polymorphs for $LiBH_4$ were also adapted and optimized for $NaBH_4$ and conversely.

DFPT calculations have been performed, at selected pressures, using both the PAW framework (PW cut-off 40 Ha) and ONCVPSP norm-conserving pseudopotentials (PW cut-off 50 Ha).[71] In the latter case, the structures were re-optimized using ONCVPSP pseudopotentials prior to the DFPT calculation.

The MD runs have been performed on a cell of *Pnma* $NaBH_4$ with additional hydrogen molecules, to inspect the possibility of hydrogen insertion in the borohydride, and the structure that may be formed in such conditions. MD runs in the (NPT) ensemble have been performed using a 192 atoms supercell of the disordered cubic phase V of $LiBH_4$ over more than 5000 steps in order to obtain the equation of state at 300 K. For checking purpose (NVT) MD runs have been performed using the averaged volume obtained in (NPT) MD runs, providing the right pressure with a precision of 0.3 GPa.

AIRSS was used to search for the ground state of phase VI of $LiBH_4$. The starting cell was given by the experiment. Six configurations were first generated with a random distribution of lithium and boron atoms. Then, four hydrogen atoms were randomly placed inside a shell around each boron atom. A total of 34 random configurations with 24 atoms were optimized by DFT at 68 GPa. This seemed sufficient to identify the crystal structure of phase VI.

Results and discussion

Pressure-induced structural changes in $NaBH_4$

A previous Raman study of $NaBH_4$ under pressure up to 30 GPa suggested that a new phase transition to a possible monoclinic α-$LiAlH_4$ ($P2_1/c$)-type phase occurred at 14 GPa.[32] To confirm this hypothesis, the Raman stretching modes of the B–H bonds were measured up to 60 GPa. The corresponding background-corrected spectra are represented in Fig. 1 along with the pressure evolution of the vibrons of the *Pnma* phase. Six peaks can be clearly followed up to 30 GPa but the signal becomes broader as the pressure increased, making the determination of the peak position less accurate even with the subtraction of the second-order contribution of the diamond. Nevertheless, the six peaks, sometimes in the forms of shoulders, have been followed up to 60 GPa. The evolution of their frequencies is sub-linear as a function of pressure and no new peak seems to emerge, in contrast to George *et al.*'s suggestion.[32] It has to be noted that the broadening of the Raman lines is probably due to non-hydrostaticity, as the Raman spectra in George *et al.*'s study

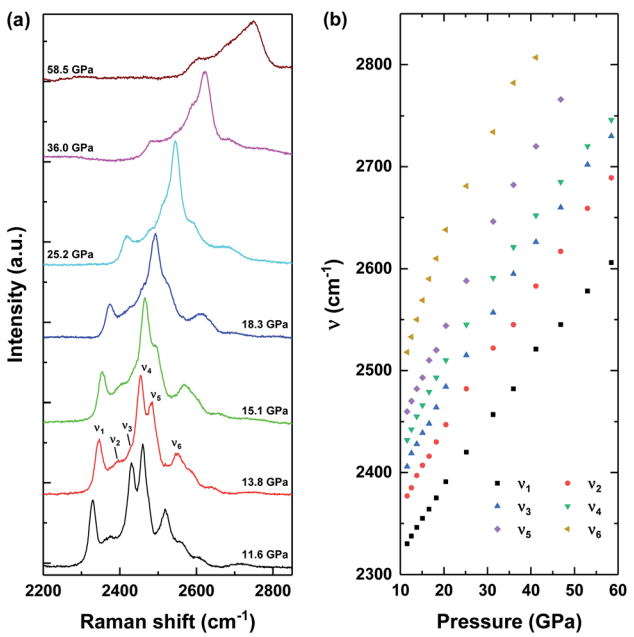

Fig. 1 (a) Raman spectra of high pressure *Pnma* $NaBH_4$ as a function of pressure (neon as a pressure medium). (b) Corresponding pressure evolution of the six Raman peaks related to B–H stretching vibrations.

are broader than ours from 12 GPa on. Hence, from the Raman measurements alone, it is not possible to confirm the existence of a phase transition above 20 GPa.

Diffraction on the *Pnma* phase had been already performed with silicone fluid as a pressure medium up to 30 GPa by Kumar *et al.*[28] and also by Filinchuk *et al.*[30] who decompressed it down to 7 GPa. We extended the X-ray diffraction study of $NaBH_4$ up to 70 GPa in neon pressure transmitting medium. Our measurements are in very good agreement with both the already published data and with the calculated equation of state of the *Pnma* phase, as can be seen in Fig. 2a. A *Vinet* adjustment of a combination of the present data and the already published data gives a bulk modulus of 19.6 GPa with its pressure derivative of 4.6 and a volume at atmospheric pressure of 56.5 $Å^3$. Fig. 2b presents a Le Bail refinement of the $NaBH_4$ diffraction pattern in the *Pnma* phase under hydrogen at 63 GPa.

Infrared absorption spectroscopy was carried out above 60 GPa and three IR bands centred around 3000 cm^{-1} corresponding to the B–H stretching modes have been followed up to 190 GPa (see ESI, Fig. S1†). Their evolution is linear when the pressure increases, which tends to show that no new phase transition nor decomposition occur under very high pressure. After structural optimizations of all the polymorphs tested, the observed phase II to phase III transition pressure could be numerically reproduced. The *Pnma* phase remained stable up to 474 GPa, above which $NaBH_4$ is predicted to metallize in a new *C*2/*c* structure (Fig. 3). This structure appeared during pressure-

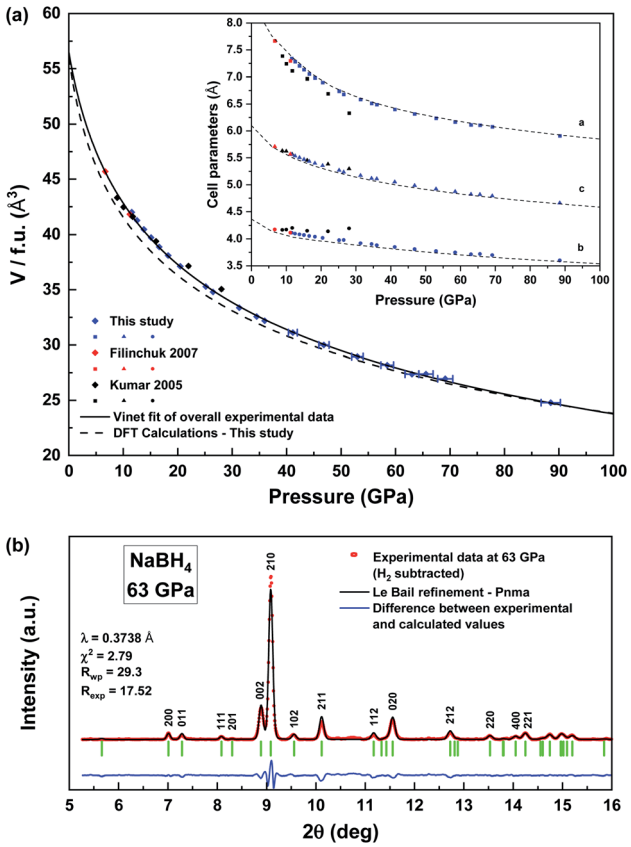

Fig. 2 (a) Experimental and calculated equations of state of *Pnma* $NaBH_4$ along with the evolution of the corresponding cell parameters under pressure (inset). The parameters of the *Vinet* fits for experimental and calculated data are respectively: $K_0 = 19.6$ & 15.7 GPa; $K'_0 = 4.6$ & 5.2; $V_0 = 56.5$ & 56.1 $Å^3$. Error bars smaller than or equal to the symbol size if not shown. (b) Le Bail refinement of the recorded diffraction pattern at 63 GPa in hydrogen ($a = 6.11$ Å, $b = 3.71$ Å, $c = 4.82$ Å).

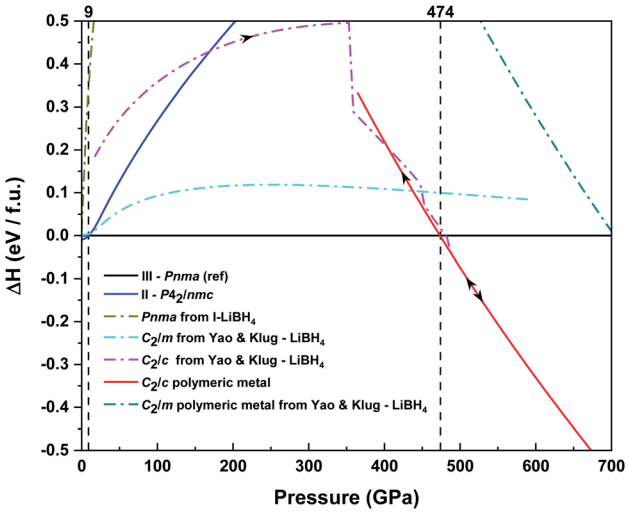

Fig. 3 Enthalpy difference per formula unit as a function of pressure for various $NaBH_4$ polymorphs. The *Pnma* $NaBH_4$ structure is taken as a reference. A solid line indicates a stable polymorph. The black arrows indicate if the structure was optimized under increasing or decreasing pressure. The $I4_1/acd$ structure adapted from phase III of $LiBH_4$ (not shown here) was also optimized at low pressure (<10 GPa) and was found to be very unstable in this pressure range. Structural optimization of the structure adapted from *C*2/*c* $LiBH_4$ gave rise to a new structure during pressure increase. This new polymorph was then optimized under decreasing pressure and turned out to be of polymeric and metallic type.

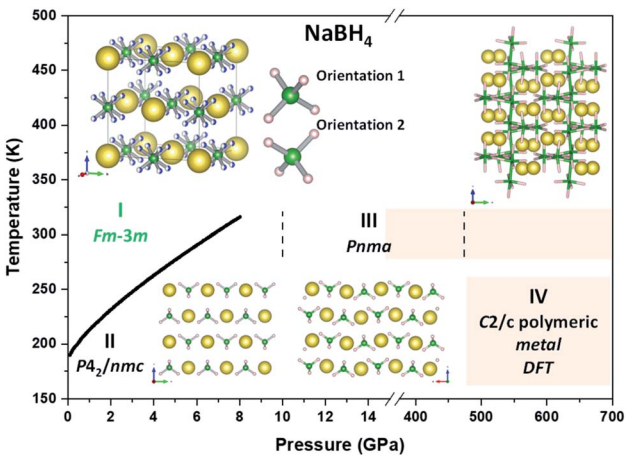

Fig. 4 Temperature *vs.* pressure phase diagram of $NaBH_4$ adapted and completed from Sundqvist.[40] Green writing indicates a phase with disorder caused by tetrahedral reorientation. Na, B and H atoms are respectively represented by yellow, green and pink spheres. Beige background indicates the new high pressure phase diagram proposed by this work.

increasing optimization of the adapted non-metallic $C2/c$ $LiBH_4$ polymorph found by Yao & Klug.[51] This metallic sodium borohydride has a polymeric/layered feature without any more tetrahedral (see ESI, Fig. S5†). Each boron & hydrogen-containing layer is made of zigzag chains linked between them by a B_{chain1}–H–B–H–B_{chain2} link. Each chain is composed by a pattern which alternates simple B–B bonds and B–2H–B bonds as in diborane(6) or maybe as in diborane(4) (plus terminal hydrogen atoms).

The phase diagram of $NaBH_4$ can thus be extended and a new one is presented in Fig. 4.

Pressure-induced structural changes in $LiBH_4$

X-ray diffraction was performed on $LiBH_4$ embedded in helium as a hydrostatic pressure medium. As can be seen in Fig. 5, the transition pressures and measured volumes are in good agreement with Nakano *et al.*'s previous study.[46] Even the intermediate disordered phase V′ appears, while it was hypothesised that it would appear only in non-hydrostatic conditions. The volume of the disordered cubic phase V was also calculated by averaging the volume over the equilibrated isothermal–isobaric MD trajectories at 300 K and several pressures. This calculated volume agrees well with the experimental data within the experimental error. Starting from 45 GPa, the recorded X-ray signal of the cubic phase V slowly decreases in intensity as already seen by Nakano *et al.*[46] and new peaks of a phase VI start to emerge. A first run with 300 μm culets leads to a mixture of phase V and VI up to 72 GPa, the highest pressure achieved in this run. The mixture was confirmed by Raman spectroscopy. The six new peaks detected at this pressure were not sufficient to determine a plausible cell for the new phase VI. Therefore, X-ray diffraction was then performed with a more sensitive detector (mar555) on the cell that was used for the Raman study here after. At 68 GPa, the $LiBH_4$ sample without pressure medium was found totally transformed into phase VI and an orthorhombic cell containing four $LiBH_4$ unit formula can be inferred from the first eleven reflections seen in the image plate (up to $2\theta = 16°$). The highest angle peaks are broad and weak but could also be described by this orthorhombic cell. As can be seen in (Fig. 5a), this cell corresponds to the computed *Pnma* phase VI with the same structure as the $NaBH_4$ *Pnma* phase III. This structure is calculated to be thermodynamically stable from 29 GPa in comparison to the $I4_1/acd$ structure and not the disordered $Fm\bar{3}m$ phase V. Besides, to be sure of the hydrogen atoms orientation, more than thirty random draws of the atoms inside the experimental cell followed by structural optimization gave the $NaBH_4$-like *Pnma* structure as the most stable configuration. Besides, the apparition of this phase for $LiBH_4$ just after the $Fm\bar{3}m$ disordered phase V is logical, as the structure is only a pressure-distorted version of the $P4_2/nmc$ phase II of $NaBH_4$ which appears right after the same disordered $Fm\bar{3}m$ phase I of $NaBH_4$.

The X-ray study was completed by a second run in helium with a much smaller sample and a 100 μm culet, three peaks could be followed up to 130 GPa and have allowed us to extend the PV equation of state of $LiBH_4$ at room temperature. At

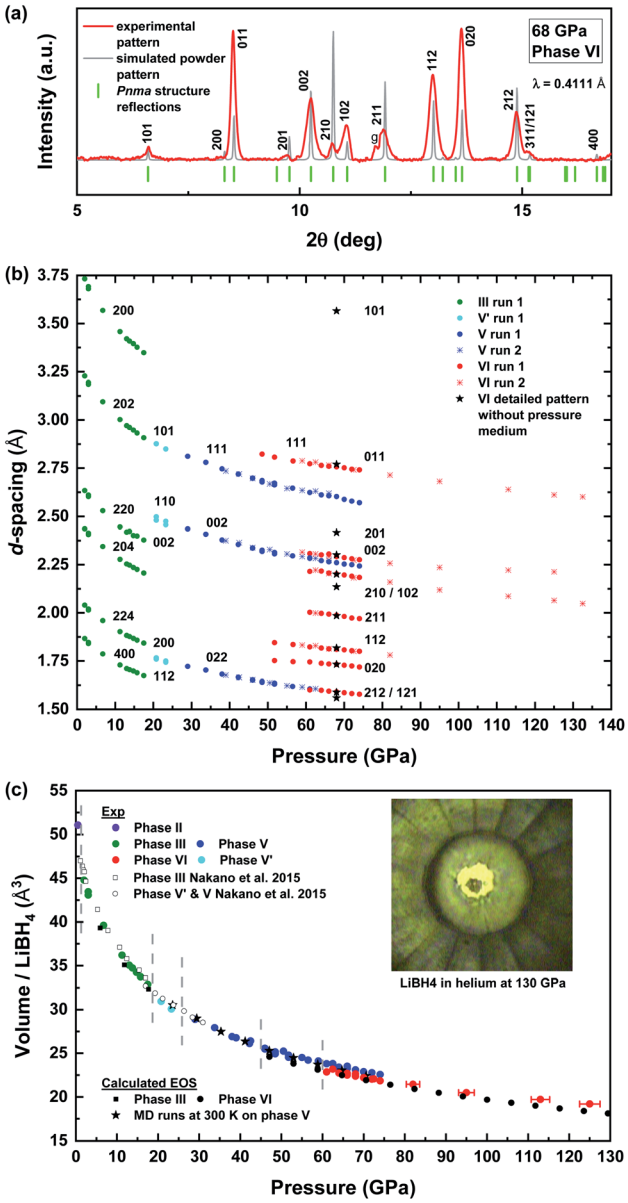

Fig. 5 (a) Diffraction pattern of the new phase VI recorded at 68 GPa without pressure medium along with a simulated powder pattern of the corresponding *Pnma* structure ($a = 5.67$ Å, $b = 4.60$ Å, $c = 3.46$ Å). "g" stands for gasket. The sample was not in a sufficient powder state to perform Rietveld refinement. (b) *d*-Spacing evolution in pressure for each phase of $LiBH_4$. (c) Experimental and calculated equation of state of $LiBH_4$ up to 130 GPa. Vertical grey lines materialize the pressure region of the phase diagram given in Fig. 9. All data points here were taken on $LiBH_4$ under hydrostatic condition in helium which seems to favour the persistence of the disordered phase V above 60 GPa. The parameters of the *Vinet* fit for phase III are: $K_0 = 25$ GPa; $K'_0 = 3.4$; $V_0 = 48$ Å^3. For the sake of clarity, pressure error bars are only shown for data points above 80 GPa (volume error bars smaller than the symbol size).

74 GPa, the volume drops between phase V and the new phase VI is around 3%.

Typical Raman spectra without pressure medium are presented in Fig. 6. A striking quasi disappearance of the low

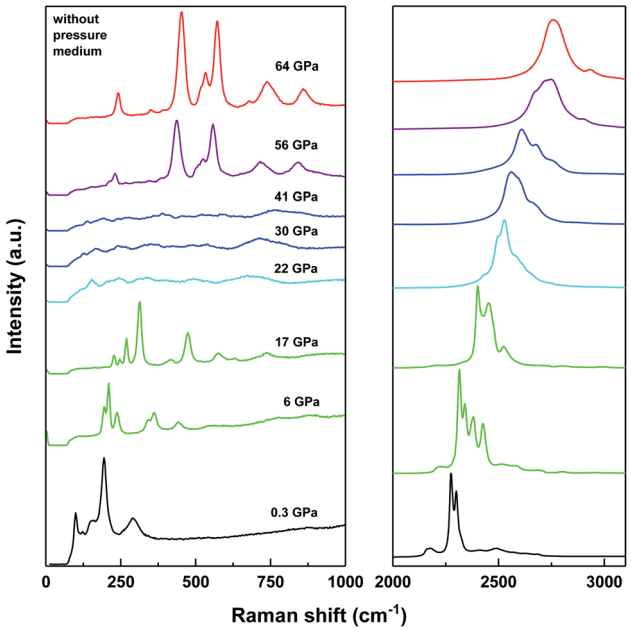

Fig. 6 Raman spectra of $LiBH_4$ at selected pressures and 300 K (no pressure medium). Each different colour corresponds to a $LiBH_4$ phase. Black: *Pnma* – phase II; green: $I4_1/acd$ – phase III; light-blue: disordered tetragonal $I4/mmm$ – phase V′; blue: disordered cubic $Fm\bar{3}m$ – phase V; violet: mixture between phase V and VI; red: orthorhombic *Pnma* – phase VI.

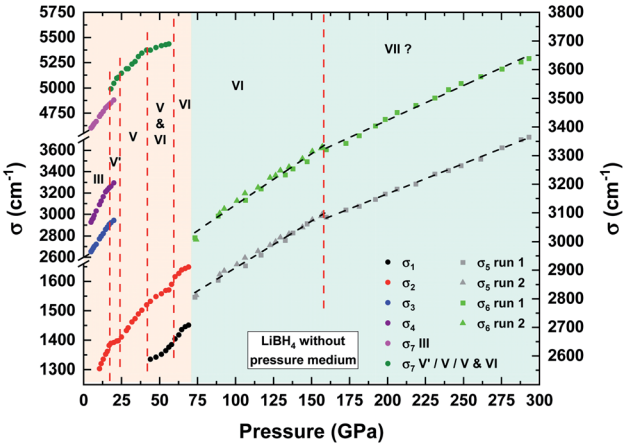

Fig. 7 Infrared frequencies *versus* pressure for $LiBH_4$ without any pressure medium (only a few absorption bands could be followed). The *Y* axis of the data in red background is on the left (corresponding to a single run with 300 μm culets) and the *Y* axis of the data in green background is on the right (corresponding to two runs with 40 μm culets). The two bands followed with the 40 μm culets were saturated with the 300 μm culets. No pressure medium was used. Band no. 4 added (it was missing but presented in Fig. S3†).

frequency modes is recorded from 20 GPa on, when $LiBH_4$ transforms from an ordered tetragonal $I4_1/acd$ phase III to two disordered phases: a tetragonal and then a cubic phase (phases V′ and V). As the pressure increases, new low frequency vibrons start to appear at 45 GPa and are well defined near 55 GPa. Nevertheless, at this pressure, the Raman stretching modes in the 2500 cm^{-1} region indicate that a fraction of the cubic phase remains, as three peaks are distinguishable whereas from 64 GPa on, only two peaks are distinguishable. Hence Raman spectra clearly indicate a reordering of the $[BH_4]^-$ tetrahedron leading to the new high pressure phase VI of $LiBH_4$.

The infrared absorption study presented in Fig. 7 confirms the appearance of this new phase as well and has allowed us to extend the study $LiBH_4$ under higher pressure. As can be seen, the transition between phase III and phase V′/V is clearly indicated by the disappearance of the denoted σ_3 absorption band and a clear slope change in the evolution of the denoted σ_2 (corresponding to a bending mode[72]) starting from 17 GPa. Other slope changes for σ_2 occur: (1) near 25 GPa, indicating the complete transformation of the disordered tetragonal phase V′ into the disordered phase V, (2) near 45 GPa, corresponding to the coexistence zone between phase V and VI and (3) above 60 GPa, interpreted as the corresponding starting pressure at which only phase VI is present.

Higher pressure IR absorption study up to 290 GPa was also conducted with a 40 μm DAC by following the two main stretching bands which were saturated in the experiment with the 300 μm culet. A slight slope jump and a slope change are detected at 160 GPa which could be a very first indicator of a new phase transition to a potential phase VII (see Fig. S2 and S3 in ESI† for IR spectra). Should it be confirmed by XRD, this phase VII would probably not be one of the phases predicted by Yao & Klug, *i.e.* monoclinic $C2/m$ or $C2/c$ insulating phases, as they are computed to be unstable with respect to the new phase VI at this pressure (Fig. 8). One can hypothesize a slight monoclinic distortion of phase VI. At higher pressure, the insulating $C2/c$ structure proposed by Yao & Klug[51] is calculated

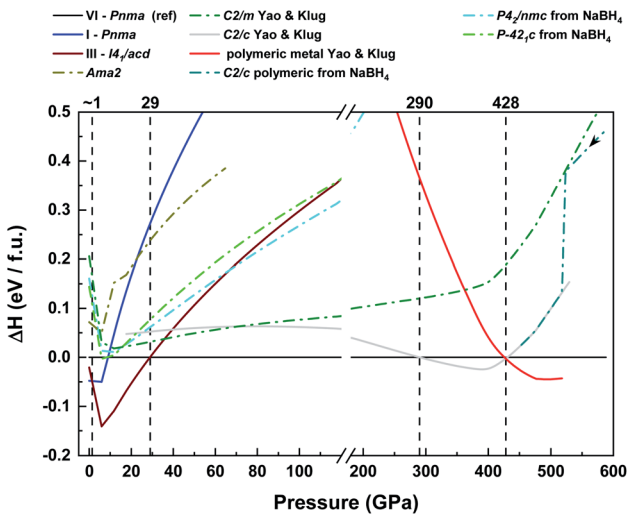

Fig. 8 Enthalpy difference per formula unit as a function of pressure for various $LiBH_4$ polymorphs. The new *Pnma* phase VI is taken as a reference. The black arrows indicate if the structure was optimized under increasing or decreasing pressure. Structural optimization of the LiBH4 phase I and of the structure adapted from $P42_1c$ NaBH4 gave rise to a new structure during pressure increase. These two new polymorphs were then optimized under decreasing pressure but none of them was found to be stable inside any pressure range.

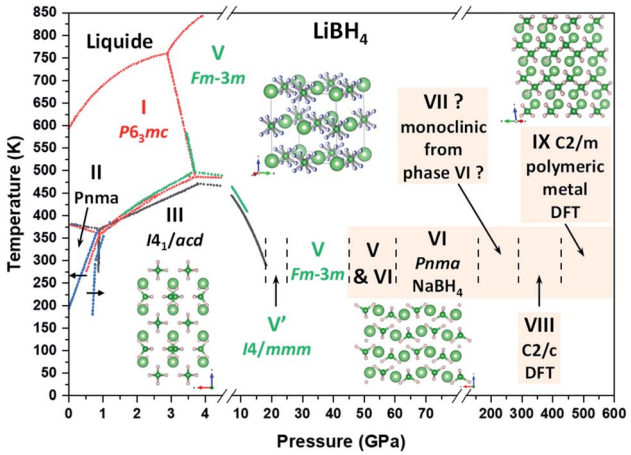

Fig. 9 Temperature *vs.* pressure phase diagram of LiBH4 adapted and completed from past studies[33,40,43,46,47,51] (dotted lines: red – Pistorius;[41] black – Dmitriev *et al.*;[43] blue – Sundqvist *et al.*;[33] green – Yamawaki *et al.*[47]). Green writing indicates a phase with disorder caused by tetrahedral reorientation. Red writing indicates a phase with disorder caused by tetrahedral rotation along one of its axes. Pressure range for the coexistence of phase V and VI is given for non-hydrostatic conditions; for helium pressure transmitting medium, this zone starts at 60 GPa and probably terminates near 80 GPa. Note that phase V′ is considered as metastable[46] and that there is unconfirmed theoretical debate for structure of phase I.[73,74] Li, B and H atoms are respectively represented by light green, dark green and pink spheres. Phase VIII and IX are the phases from Yao & Klug for which the transition pressures were recalculated. Beige background indicates the new high pressure phase diagram proposed by this work.

to become thermodynamically favourable near 290 GPa. Then, $LiBH_4$ is expected to metallize at 428 GPa by transforming into the polymeric $C2/m$ structure predicted by Yao & Klug.[51] This metallic phase, unlike the metallic phase of $NaBH_4$, does not contain B–2H–B bonds but simple B–H–B or B–B bonds.

The phase diagram of $LiBH_4$ can thus be extended and a new one is presented in Fig. 9.

Hydrogen impurities in $LiBH_4$

Infrared transmission measurements on lithium borohydride reveal the presence of a small absorption band near 4550 cm^{-1} in phase II. Its frequency is greater than the frequency of pure H_2 and corresponds to the stretching vibration of few H_2 molecules trapped inside the $LiBH_4$ crystal lattice. As far as we know, this slight amount of hydrogen inside $LiBH_4$ was never reported before; maybe because this trapped H_2 is hardly detected by Raman spectroscopy (IR absorption measurements can be much more sensitive than Raman spectroscopy to detect a hydrogen vibron). Incidentally, it should be noted that the $LiBH_4$ commercial batch was new and the glove box free of O_2/H_2O at a level inferior to 1 ppm and no water contamination was detected by IR absorption, which probably rules out a hypothetical hydrolysis reaction. Hence, the presence of H_2 is thought to be due to impurities trapped in the $LiBH_4$ structure during synthesis. Such impurities do not change the crystal structure of $LiBH_4$ and probably only marginally change its volume, measured by XRD. Indeed, the experimental structures and volumes agree fairly well with the earlier literature studies and the DFT-calculated ones (Fig. 5).

This H_2 vibron has been followed during pressure increase (band denoted σ_7 in Fig. 7). The intensity of the band increases during the transition from phase II to III (see ESI, Fig. S9†). This can be due to a higher polarisation of the H_2 molecule in phase III or a slight decomposition during the phase change, even if such decomposition is more a temperature effect (as in the phase II to the high-temperature phase I transition at ambient pressure[50]) than a pressure effect. A frequency jump near 20 GPa is correlated with the phase III to phase V′/V transformation, and the breaks in slope at higher pressure are correlated to the coexistence of phases V and VI defined above. Hence, this small amount of H_2 in the $LiBH_4$ lattice turned to be a good probe of the structural transformation under pressure. During the phase V to VI transition, the H_2 signal broadens and tends to vanish, indicating a low signal or a possible diffusion of the hydrogen into the gasket.

Hydrogen complexes with $NaBH_4$

As we have seen, $NaBH_4$ stays in its orthorhombic *Pnma* phase under high pressure which is not very interesting from a hydrogen storage perspective. Several NPT MD runs have been performed to try to find new stable $NaBH_4(H_2)_x$ complexes with high hydrogen content. The additional hydrogen was initially inserted inside the void in the $NaBH_4$ *Pnma* structure at 50 GPa. Several stoichiometries have been tested with $x = 1/2$, 1, 3/2, 2. The total number of atoms in the cell was 28. On the four stoichiometries tested, only the one with $x = 1/2$ lead to a structure compatible with a possible insertion. The resulting structure, shown in Fig. 10, was then optimized and could be described in the $P2_1/c$ space group (see ESI† for the Wyckoff

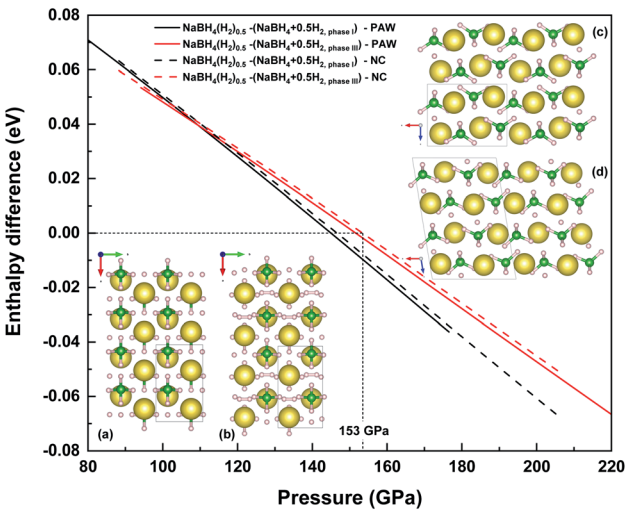

Fig. 10 Enthalpy difference between $NaBH_4$ + $0.5H_2$ and $NaBH_4(H_2)_{0.5}$ as a function of pressure. NC: Norm-Conserving method. PAW: Projector Augmented Wave method. View along the *c* axis of (a) the $NaBH_4$ *Pnma* structure and (b) the $NaBH_4(H_2)_{0.5}$ $P2_1/c$ structure. View along the *b* axis of (c) the $NaBH_4$ *Pnma* structure and (d) the $NaBH_4(H_2)_{0.5}$ $P2_1/c$ structure.

positions). The lattice of the orthorhombic *Pnma* structure was distorted into a monoclinic one due to hydrogen insertion without any major reorganisation of the atoms. In this structure, H forms a bridge between the edges of two distinct tetrahedral. By comparing the enthalpies of pure $NaBH_4 + 0.5H_2$ and $NaBH_4(H_2)_{0.5}$ as a function of pressure, we found that this new complex becomes stable above 153 GPa. For the reference phase of H_2, we have used the *C*2/c-32 phase[17] for phase I and the *C*2/c-24 phase which is the accepted candidate phase for the phase III of dense hydrogen.[75] Phonon band structures of $NaBH_4$ and $NaBH_4(H_2)_{0.5}$ at 206 GPa can be found in ESI (Fig. S7 and S8†). Note that a slight dynamical instability is observed in the case of $NaBH_4(H_2)_{0.5}$, close to the gamma point, proving that a slightly more stable structure may exist (however, its direct simulation would require the building of a supercell 10 times larger, which is currently beyond our numerical possibilities). The new compound remains an insulator and the stretching vibration frequency of the inserted H_2 molecules is higher than that of pure hydrogen by 650 cm^{-1} at 200 GPa (H_2 at 3750 cm^{-1} at 75 K and 200 GPa (ref. 76)). Experimentally, this higher vibration frequency should easily be detected thanks to Raman or IR spectroscopy. The volume is also slightly increased by 8% at 200 GPa (+1.57 $Å^3$) compared to *Pnma* $NaBH_4$. We have performed preliminary experiments on $NaBH_4$ loaded with H_2 in a DAC, and no such hints of H_2 insertion have been detected up to 88 GPa during the room temperature pressure increase, which is in agreement with the calculations.

Conclusion

The phase diagrams of both lithium and sodium borohydrides have been experimentally extended in pressure above 100 GPa and up to the metallization of these compounds by *ab initio* calculations. Their extended phase diagrams in the multi-Mbar range are shown in Fig. 9 and 4, respectively. The polymorphism of $LiBH_4$ is richer than the one of $NaBH_4$. Indeed, $LiBH_4$ is transformed under pressure into five specific polymorphs at least. Previously, only the disordered $Fm\bar{3}m$ cubic phase was known to be shared between the two compounds, but in the present study, we have found a shared high pressure *Pnma* structure. As suggested by the IR absorption data, this phase might undergo a monoclinic distortion under pressure for $LiBH_4$ but not for $NaBH_4$.

Moreover, the reliability of highly converged GGA-PBE calculations has been demonstrated in this study, both by a good replication of the phase diagram of the two borohydrides but also by a successful *ab initio* search for the structure of phase VI of $LiBH_4$. Hence, machine learning/AIRSS search and design should be useful to discover new borohydrides or, more generally, new ternary hydrides for better solid hydrogen storage.

With the prediction of the stability of a new $NaBH_4(H_2)_{0.5}$ hydride under pressure, the question of the possibility of inserting more hydrogen inside alkaline borohydrides which do not have a very open metal–organic framework is raised. Moreover, the detection of trapped H_2 inside the polymorphs of $LiBH_4$ under pressure calls for new numerical and experimental searches for $LiBH_4(H_2)_x$ complexes with high hydrogen content, as what was done for $NaBH_4$, especially in phase VI which is shared between the two compounds.

Conflicts of interest

There are no conflicts to declare.

Acknowledgements

We would like to very warmly thank Paul Dumas for his help on SMIS beamline and also Mrs Stéphanie Blanchandin and Mrs Karine Chaouchi for their precious help with the glovebox at the Soleil Synchrotron.

Notes and references

1 P. Martelli, R. Caputo, A. Remhof, P. Mauron, A. Borgschulte and A. Züttel, *J. Phys. Chem. C*, 2010, **114**, 7173–7177.
2 A. Züttel, S. Rentsch, P. Fischer, P. Wenger, P. Sudan, P. Mauron and C. Emmenegger, *J. Alloys Compd.*, 2003, **356–357**, 515–520.
3 A. Züttel, A. Borgschulte and S. I. Orimo, *Scr. Mater.*, 2007, **56**, 823–828.
4 J. Manna, M. Vashistha and P. Sharma, *Int. J. Energy a Clean Environ.*, 2010, **11**, 65–97.
5 I. Saldan, *Open Chem*, 2011, **9**, 761–775.
6 L. H. Rude, T. K. Nielsen, D. B. Ravnsbaek, U. Bösenberg, M. B. Ley, B. Richter, L. M. Arnbjerg, M. Dornheim, Y. Filinchuk, F. Besenbacher and T. R. Jensen, *Phys. status solidi*, 2011, **208**, 1754–1773.
7 M. L. Christian and K.-F. Aguey-Zinsou, *ACS Nano*, 2012, **6**, 7739–7751.
8 M. B. Ley, L. H. Jepsen, Y. Lee, Y. W. Cho, J. M. Bellosta von Colbe, M. Dornheim, M. Rokni, J. O. Jensen, M. Sloth, Y. Filinchuk, J. E. Jørgensen, F. Besenbacher and T. R. Jensen, *Mater. Today*, 2014, **17**, 122–128.
9 J. Mao and D. Gregory, *Energies*, 2015, **8**, 430–453.
10 M. Paskevicius, L. H. Jepsen, P. Schouwink, R. Černý, D. B. Ravnsbæk, Y. Filinchuk, M. Dornheim, F. Besenbacher and T. R. Jensen, *Chem. Soc. Rev.*, 2017, **46**, 1565–1634.
11 Y. Song, *Phys. Chem. Chem. Phys.*, 2013, **15**, 14524–14547.
12 V. Ban, A. V. Soloninin, A. V. Skripov, J. Hadermann, A. Abakumov and Y. Filinchuk, *J. Phys. Chem. C*, 2014, **118**, 23402–23408.
13 N. A. Tumanov, E. Roedern, Z. Łodziana, D. B. Nielsen, T. R. Jensen, A. V. Talyzin, R. Černý, D. Chernyshov, V. Dmitriev, T. Palasyuk and Y. Filinchuk, *Chem. Mater.*, 2016, **28**, 274–283.
14 M. A. Rafiee, *Phys. Chem. Res.*, 2018, **6**, 657–666.
15 A. Marizy, G. Geneste, P. Loubeyre, B. Guigue and G. Garbarino, *Phys. Rev. B*, 2018, **97**, 184103.
16 C. M. Pépin, A. Dewaele, G. Geneste, P. Loubeyre and M. Mezouar, *Phys. Rev. Lett.*, 2014, **113**, 265504.
17 C. M. Pépin, G. Geneste, A. Dewaele, M. Mezouar and P. Loubeyre, *Science*, 2017, **357**, 382–385.

18 R. S. Chellappa, M. Somayazulu, V. V. Struzhkin, T. Autrey and R. J. Hemley, *J. Chem. Phys.*, 2009, **131**, 224515.
19 Y. Lin, E. Welchman, T. Thonhauser and W. L. Mao, *J. Mater. Chem. A*, 2017, **5**, 7111–7117.
20 A. M. Soldate, *J. Am. Chem. Soc.*, 1947, **69**, 987.
21 W. H. Stockmayer and C. C. Stephenson, *J. Chem. Phys.*, 1953, **21**, 1311–1312.
22 S. C. Abrahams and J. Kalnajs, *J. Chem. Phys.*, 1954, **22**, 434–436.
23 R. L. Davis and C. H. L. Kennard, *J. Solid State Chem.*, 1985, **59**, 393–396.
24 A. Remhof, Z. Łodziana, P. Martelli, O. Friedrichs, A. Züttel, A. Skripov, J. Embs and T. Strässle, *Phys. Rev. B: Condens. Matter Mater. Phys.*, 2010, **81**, 1–9.
25 D. G. Allis and B. S. Hudson, *Chem. Phys. Lett.*, 2004, **385**, 166–172.
26 P. Fischer and A. Züttel, *Mater. Sci. Forum*, 2004, **443–444**, 287–290.
27 C. M. Araújo, R. Ahuja, a. V. Talyzin and B. Sundqvist, *Phys. Rev. B: Condens. Matter Mater. Phys.*, 2005, **72**, 1–5.
28 R. S. Kumar and A. L. Cornelius, *Appl. Phys. Lett.*, 2005, **87**, 261916.
29 B. Sundqvist and O. Andersson, *Phys. Rev. B: Condens. Matter Mater. Phys.*, 2006, **73**, 2005–2007.
30 Y. Filinchuk, A. V. Talyzin, D. Chernyshov and V. Dmitriev, *Phys. Rev. B: Condens. Matter Mater. Phys.*, 2007, **76**, 7–10.
31 E. Kim, R. Kumar, P. F. Weck, A. L. Cornelius, M. Nicol, S. C. Vogel, J. Zhang, M. Hartl, A. C. Stowe, L. Daemen and S. Carolina, *J. Phys. Chem. B*, 2007, **111**, 13873–13876.
32 L. George, V. Drozd, H. Couvy, J. Chen and S. K. Saxena, *J. Chem. Phys.*, 2009, **131**, 1–7.
33 B. Sundqvist and O. Andersson, *Int. J. Thermophys.*, 2009, **30**, 1118–1129.
34 G. Lee, J.-Y. Lee and J. S. Kim, *Solid State Commun.*, 2006, **139**, 516–521.
35 F. Yu, J.-X. Sun, R.-G. Tian, G.-F. Ji and W.-J. Zhu, *Chem. Phys.*, 2009, **362**, 135–139.
36 R. Caputo, A. Tekin, W. Sikora and A. Züttel, *Chem. Phys. Lett.*, 2009, **480**, 203–209.
37 C. Y. Zhu, Y. H. Liu, F. B. Tian and T. Cui, *Phys. Status Solidi B*, 2011, **248**, 1139–1142.
38 Y. Filinchuk, D. Chemyshov and V. Dmitriev, *Zeitschrift fur Krist*, 2008, **223**, 649–659.
39 R. Caputo and A. Tekin, *J. Solid State Chem.*, 2012, **190**, 310.
40 B. Sundqvist, *Solid State Phenom*, 2009, **150**, 175–195.
41 C. W. F. T. Pistorius, *Zeitschrift für Phys. Chemie*, 1974, **88**, 253–263.
42 A. V. Talyzin, O. Andersson, B. Sundqvist, A. Kurnosov and L. Dubrovinsky, *J. Solid State Chem.*, 2007, **180**, 510–517.
43 V. Dmitriev, Y. Filinchuk, D. Chernyshov, A. V. Talyzin, A. Dzwilevski, O. Andersson, B. Sundqvist and A. Kurnosov, *Phys. Rev. B: Condens. Matter Mater. Phys.*, 2008, **77**, 1–11.
44 Y. Filinchuk, D. Chernyshov and R. Cerny, *J. Phys. Chem. C*, 2008, **112**, 10579–10584.
45 Y. Filinchuk, D. Chernyshov, A. Nevidomskyy and V. Dmitriev, *Angew. Chem., Int. Ed.*, 2008, **47**, 529–532.
46 S. Nakano, H. Fujihisa, H. Yamawaki and T. Kikegawa, *J. Phys. Chem. C*, 2015, **119**, 3911–3917.
47 H. Yamawaki, H. Fujihisa, Y. Gotoh and S. Nakano, *J. Phys. Chem. Solids*, 2015, **76**, 40–44.
48 J.-P. Soulié, G. Renaudin, R. Černý and K. Yvon, *J. Alloys Compd.*, 2002, **346**, 200–205.
49 M. R. Hartman, J. J. Rush, T. J. Udovic, R. C. Bowman and S. J. Hwang, *J. Solid State Chem.*, 2007, **180**, 1298–1305.
50 A. Züttel, P. Wenger, S. Rentsch, P. Sudan, P. Mauron and C. Emmenegger, *J. Power Sources*, 2003, **118**, 1–7.
51 Y. Yao and D. D. Klug, *Phys. Rev. B: Condens. Matter Mater. Phys.*, 2012, **86**, 064107.
52 B. Sundqvist, A. V. Talyzin and O. Andersson, *MRS Proc*, 2006, **971**, Z07–Z03.
53 K. Miwa, N. Ohba, S. Towata, Y. Nakamori and S. Orimo, *Phys. Rev. B: Condens. Matter Mater. Phys.*, 2004, **69**, 245120.
54 Z. Łodziana and T. Vegge, *Phys. Rev. Lett.*, 2004, **93**, 145501.
55 T. J. Frankcombe, G.-J. Kroes and A. Züttel, *Chem. Phys. Lett.*, 2005, **405**, 73–78.
56 P. Vajeeston, P. Ravindran, A. Kjekshus and H. Fjellvåg, *J. Alloys Compd.*, 2005, **387**, 97–104.
57 A. Tekin, R. Caputo and A. Züttel, *Phys. Rev. Lett.*, 2010, **104**, 215501.
58 S. Li, X. Ju and C. Wan, *Int. J. Hydrogen Energy*, 2014, **39**, 9330–9338.
59 M. Santhosh and R. Rajeswarapalanichamy, *J. Phys. Chem. Solids*, 2016, **88**, 68–77.
60 T. Ghellab, Z. Charifi, H. Baaziz, K. Bouferrache and B. Hamad, *Int. J. Energy Res.*, 2019, **43**, 3653–3667.
61 E. Tetik and U. Erdiven, *Chin. J. Physiol.*, 2019, **59**, 585–590.
62 C. Prescher and V. B. Prakapenka, *High Press. Res.*, 2015, **35**, 223–230.
63 J. Rodríguez-Carvajal, *Phys. B*, 1993, **192**, 55–69.
64 P. Loubeyre, F. Occelli and P. Dumas, *Phys. Rev. B: Condens. Matter Mater. Phys.*, 2013, **87**, 134101.
65 Y. Akahama and H. Kawamura, *J. Appl. Phys.*, 2006, **100**, 043516.
66 J. P. Perdew, K. Burke and M. Ernzerhof, *Phys. Rev. Lett.*, 1996, **77**, 3865–3868.
67 X. Gonze, G.-M. Rignanese, M. Verstraete, J.-M. Beuken, Y. Pouillon, R. Caracas, F. Jollet, M. Torrent, G. Zerah, M. Mikami, P. Ghosez, M. Veithen, J.-Y. Raty, V. Olevano, F. Bruneval, L. Reining, R. Godby, G. Onida, D. R. Hamann and D. C. Allan, *Zeitschrift für Krist. –Cryst. Mater.*, 2005, **220**, 558–562.
68 X. Gonze, *Phys. Rev. B: Condens. Matter Mater. Phys.*, 1997, **55**, 10337–10354.
69 X. Gonze and C. Lee, *Phys. Rev. B: Condens. Matter Mater. Phys.*, 1997, **55**, 10355–10367.
70 C. J. Pickard and R. J. Needs, *J. Phys. Condens. Matter*, 2011, **23**, 053201.
71 D. R. Hamann, *Phys. Rev. B: Condens. Matter Mater. Phys.*, 2013, **88**, 085117.
72 V. D'Anna, A. Spyratou, M. Sharma and H. Hagemann, *Spectrochim. Acta Part A Mol. Biomol. Spectrosc.*, 2014, **128**, 902–906.

73 S. A. Shevlin, C. Cazorla and Z. X. Guo, *J. Phys. Chem. C*, 2012, **116**, 13488–13496.
74 D. T. Shane, R. C. Bowman and M. S. Conradi, *J. Phys. Chem. C*, 2009, **113**, 5039–5042.
75 C. J. Pickard and R. J. Needs, *Nat. Phys.*, 2007, **3**, 473–476.
76 P. Loubeyre, F. Occelli and R. LeToullec, *Nature*, 2002, **416**, 613–617.